Electronic Supplementary Material (ESI) for Journal of Materials Chemistry A.

Template-free synthesis of novel, highly-ordered 3D hierarchical $Nb_3O_7(OH)$ superstructures with semiconductive and photoactive properties

Sophia B. Betzler,[a] Andreas Wisnet,[a] Benjamin Breitbach,[b] Christoph Mitterbauer,[c] Jonas Weicker,[d] Lukas Schmidt-Mende[d] and Christina Scheu[a†],

[a] Department of Chemistry, Ludwig-Maximilians-Universität and Center of NanoScience (CeNS), Butenandtstraße 11, 81377 Munich, Germany.
[b] Max-Planck Institut für Eisenforschung, Max-Planck-Straße 1, 40237 Düsseldorf, Germany.
[c] FEI company, Achtseweg Noord 5, 5600 KA Eindhoven, The Netherlands.
[d] Department of Physics, University of Konstanz, Universitätsstraße 10, 78464 Konstanz, Germany.

† present address: Prof. Dr. Christina Scheu, Max-Planck Institut für Eisenforschung, Max-Planck-Straße 1, 40237 Düssel dorf, Germany.

1. Quantitative analysis of the cube size

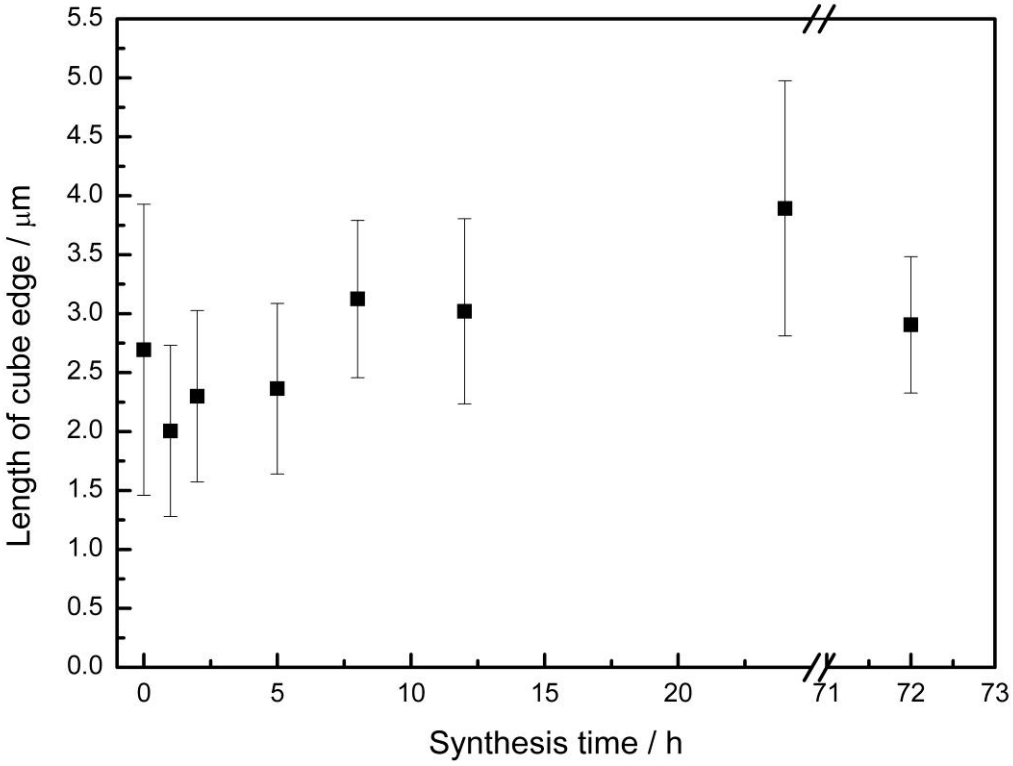

Figure S1. Quantitative analysis of the cube size in dependence of the duration of the hydrothermal synthesis. The edges of 60 cubes were measured from SEM images and averaged for the different growth states.

2. Determination of the band gap from UV/Vis Spectra

The band gaps were determined for all growth times using UV/Vis data based Tauc plots according to Equation S1[1]

$$ahv = A(hv - E_g)^{m/2} \quad \text{(S1)}$$

where a is the absorption coefficient, ν the frequency, h the Planck constant, A a constant and E_g the size of the band gap. The exponent m takes into account the presence of a direct (m=1) or indirect (m=2) band gap.[1] In the following the detected UV/Vis spectra and determined band gaps are summarized.

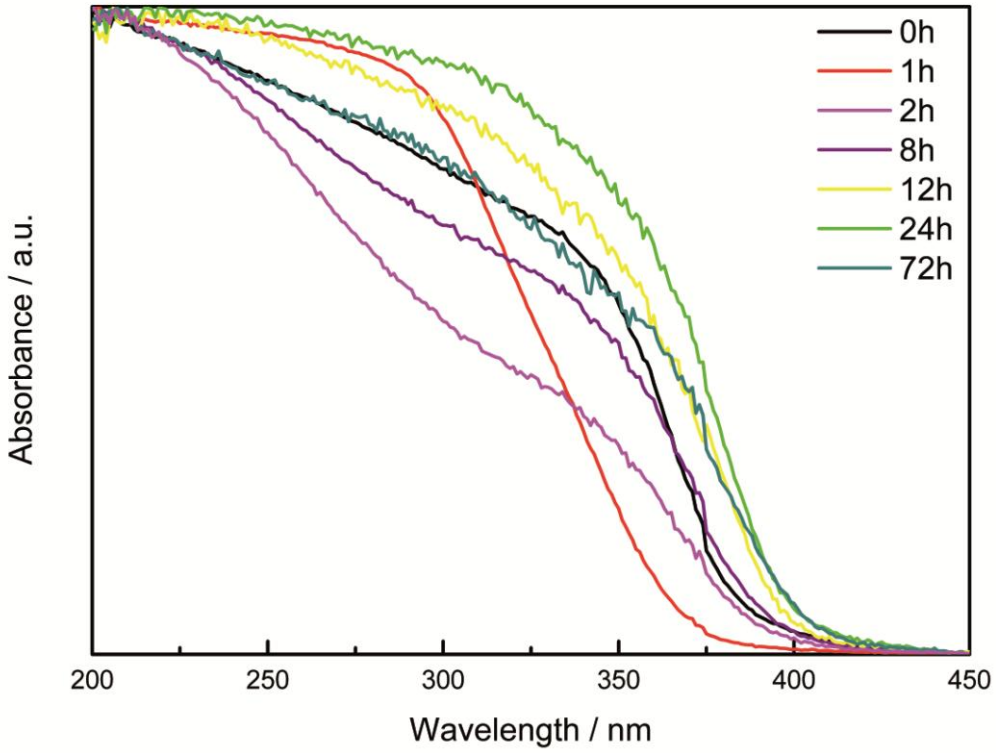

Figure S2. UV/Vis spectra detected for samples synthesized with different growth times.

Table S1. Band gaps of different growth states. The values were determined from UV/Vis spectra based Tauc plots for direct band gaps (m=1).

Growth time (h)	Band gap (eV)
0	3.30
1	3.52
2	3.28
8	3.25
12	3.21
24	3.19
72	3.16

3. Electron microscopic characterization of the nanowires and the wire network

3.1 EEL spectra detected of single nanowires

EEL spectra detected for single nanowires were compared with EEL spectra from literature,[2] at which the O-K-edge and the plasmon peaks are most significant. Figure S3 summarizes the measured data. The plasmon peak contains four characteristic features (marked as a, b, c and d), whose shape shows a better accordance with the shape reported for the plasmon of $Nb(V)_2O_5$ than with the one of $Nb(IV)O_2$. The O-K-edge consists of five features (marked as a, b, c, d and e). Again, its spectral position and shape correlates better with the data edges for Nb_2O_5 than NbO_2 stated by Bach et al..[2]

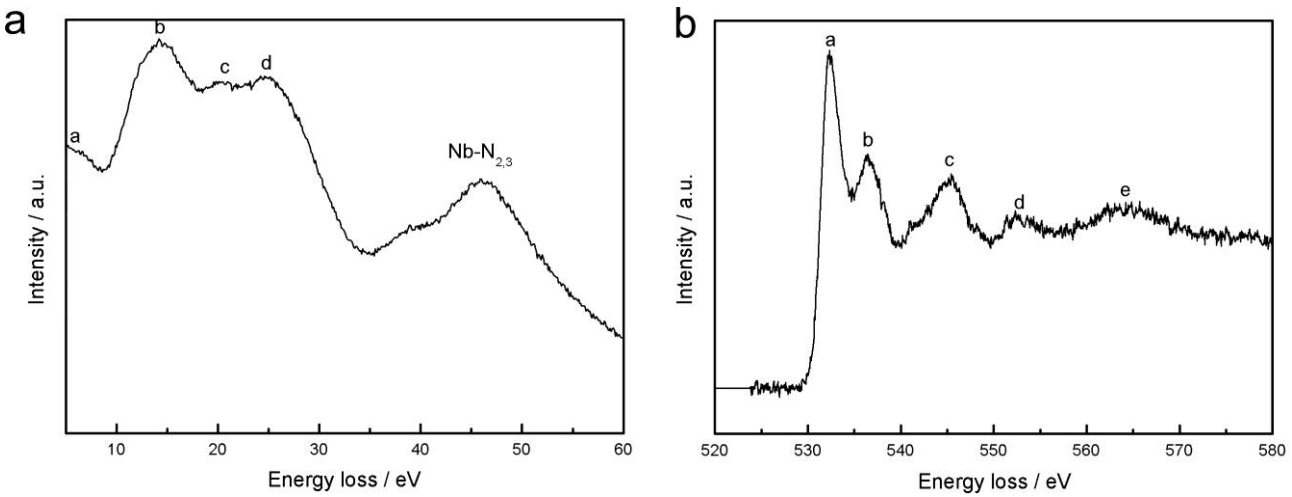

Figure S3. EELS spectra detected for cubes achieved for a synthesis time of 24 hours. a) Plasmon peak, showing four characteristic features marked as a, b, c, and d and the Nb-$N_{2,3}$-edge. b) O-K-edge, which consists of five features marked as a, b, c, d, and e.

3.2 EDX data detected of one single nanowire

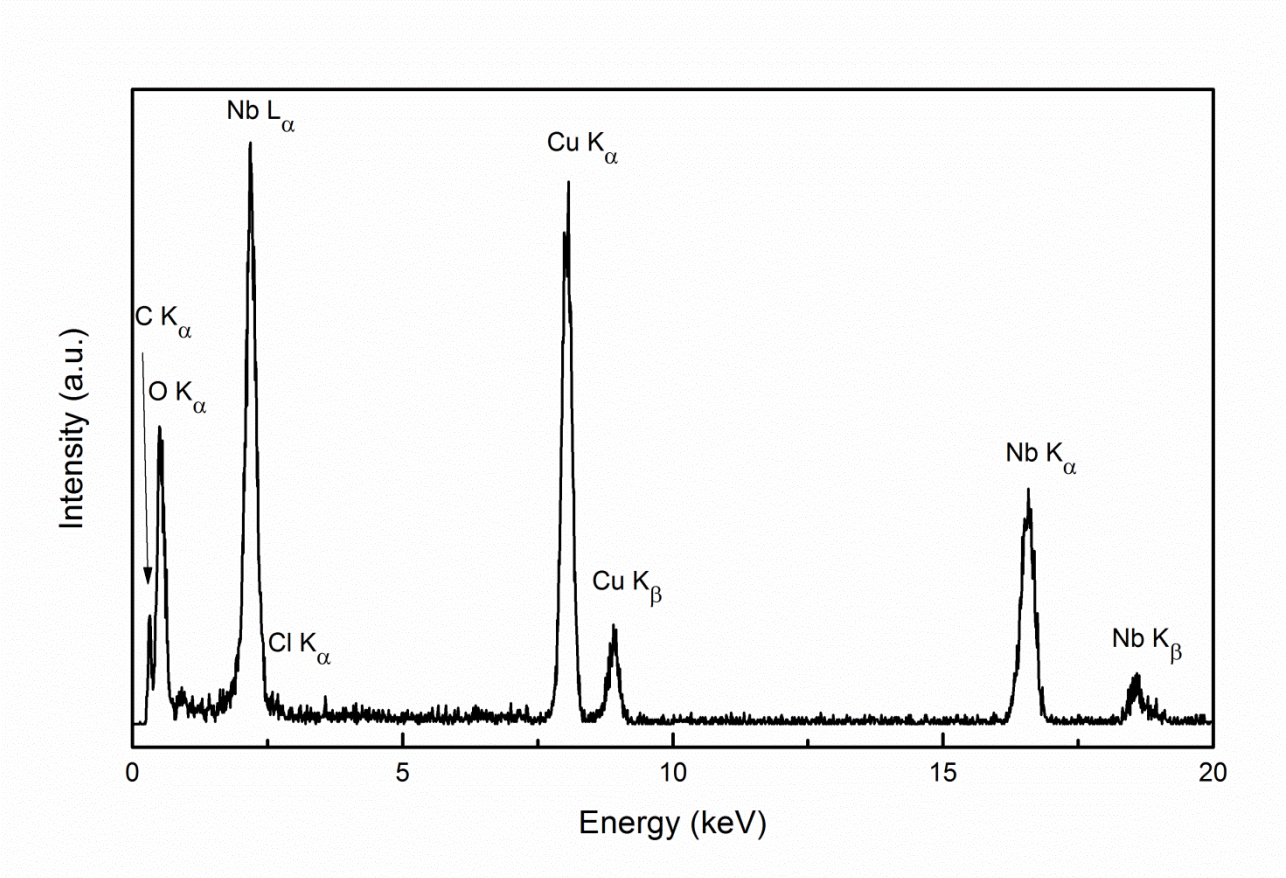

Figure S4. EDX spectra detected of one single $Nb_3O_7(OH)$ nanowire in TEM. It shows that the wires consist of niobium and oxygen and no chloride contamination is visible. In addition peaks attributable to the copper supply can be seen.

3.3 Simulations of the electron diffraction pattern

The software JEMS[3] was used to simulate the diffraction pattern achieved for distinct zone axis of $Nb_3O_7(OH)$ at an acceleration voltage of 300 kV. In Figure S5 the detected diffraction pattern and the corresponding JEMS simulation are displayed for a single nanowire lying on the carbon film and for a single nanowire of the network.

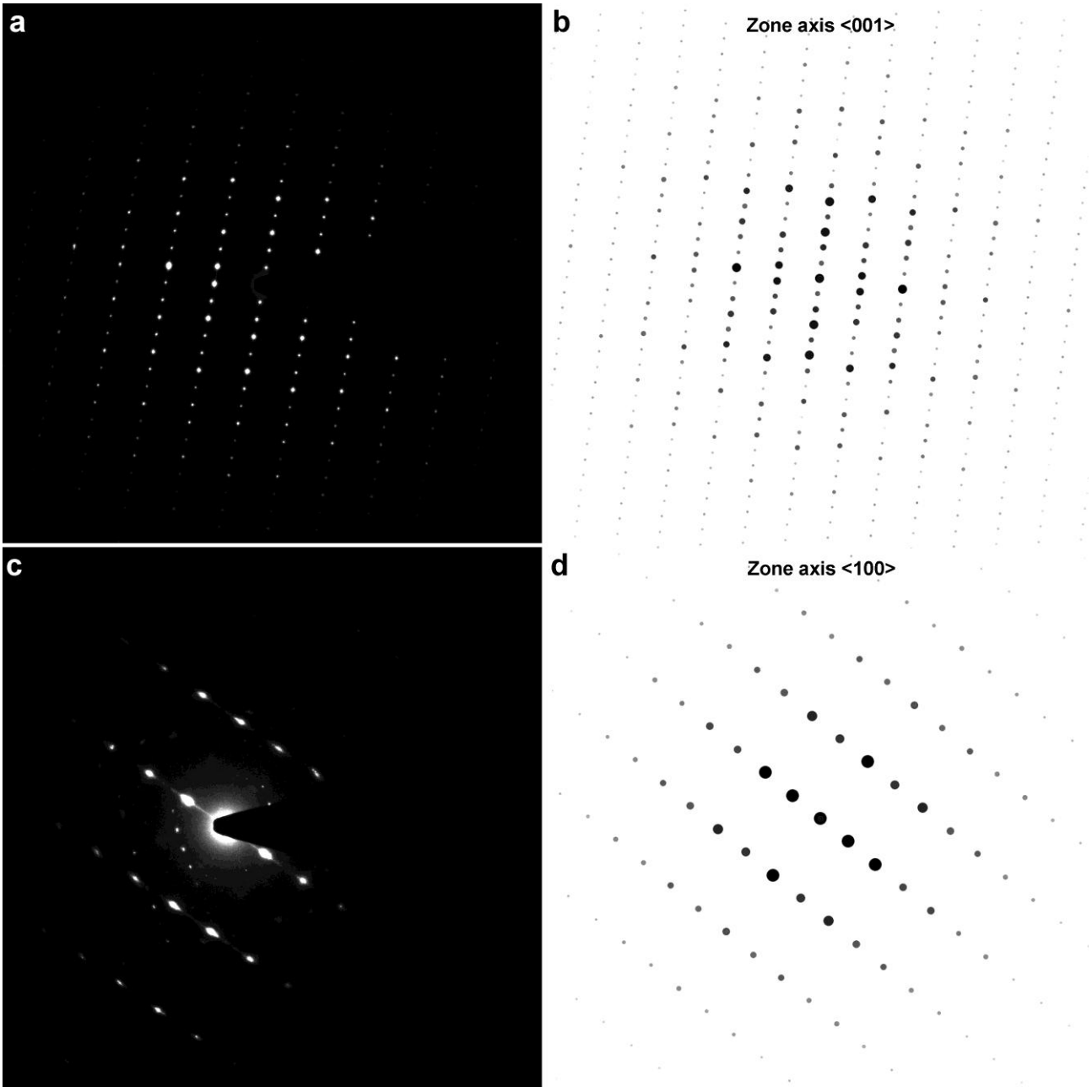

Figure S5. Experimental and simulated diffraction patterns. a)+b) electron diffraction pattern and corresponding JEMS simulation of a single nanowire lying on the carbon film. c)+d) electron diffraction pattern and JEMS simulation of a single nanowire building up the network.

3.4 Analysis of the diffraction pattern of the network

Figure S6a shows a TEM image of a network fragment and the corresponding diffraction pattern (Figure S6b). A diffraction pattern of one single nanowire of the network was used as basis for the analysis (Figure S6c). This pattern was rotated by 90° (Figure S6d) and added to the original pattern (Figure S6e). The resulting superposition coincides with the diffraction pattern detected of the network. Next to the major reflexes smaller reflexes can be seen in the diffraction pattern of the small network. These reflexes result from the underlying nanowire, which displays the <001> zone axis (marked with an arrow in Figure S6a) and does not belong to the fragment.

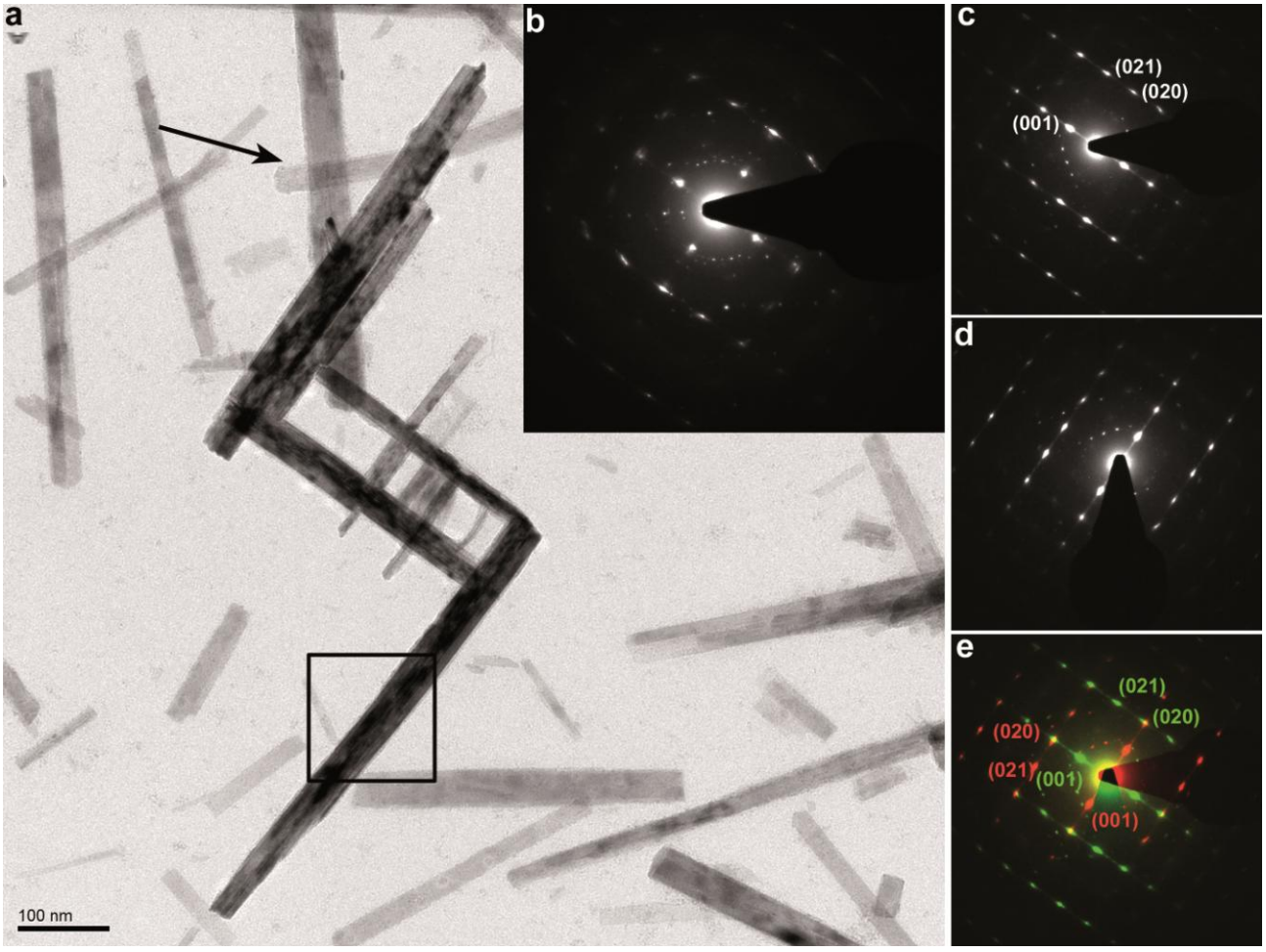

Figure S6. TEM image and electron diffraction pattern detected of a small network fragment. a) TEM image of the analyzed network fragment, which consists of nine nanowires. b) Electron diffraction pattern detected of the complete network. c) Diffraction pattern detected of one single wire, the corresponding region is marked with a black square. d) Diffraction pattern shown in c) rotated by 90°. e) Combination of the diffraction pattern shown in c) and d).

3.5 Analysis of the junctions

Using the FFT of different HRTEM images in combination with a masking tool enables the determination of the origin of the spots in the FFT via calculating the inverse FFT. The area and the corresponding spot in the FFT are colored the same (Figure S7a,b). This color-coding proves the indexing of the complex diffraction pattern of the networks, which is based on the assumption that these diffraction patterns are composed of the diffraction patterns of the distinct wires. The FFT of crossings shows additional reflexes (Figure S7b), which are not observed for T-shaped junctions (Figure S7a). The analysis indicates that these spots originate from the area where the two nanowires overlap. In addition site-specific thickness measurements were performed using both STEM and EELS. EEL spectra encode the sample thickness as the ratio of the intensity of the zero loss peak and the plasmonic region, due to the increased probability of multiple scattering events of thicker samples. The log-ratio-equation[4] (Equation S2) relates the sample thickness t with the intensities of the zero-loss peak I_0 and the total intensity of the spectrum I_t dependent on the total inelastic mean free path (MFP) of the electron in the material:

$$t = MFP \cdot \ln\left(\frac{I_t}{I_0}\right) \qquad \text{(S2)}$$

In Figure S7d,e the achieved relative thicknesses are given as numbers related to the MFP. The achieved results are proven by high angle annular dark field (HAADF)-STEM investigations, as thicker region cause a higher brightness in the images (Figure S7c). In addition HAADF images show the preservation of the atomic columns at the junction (Figure S7f).

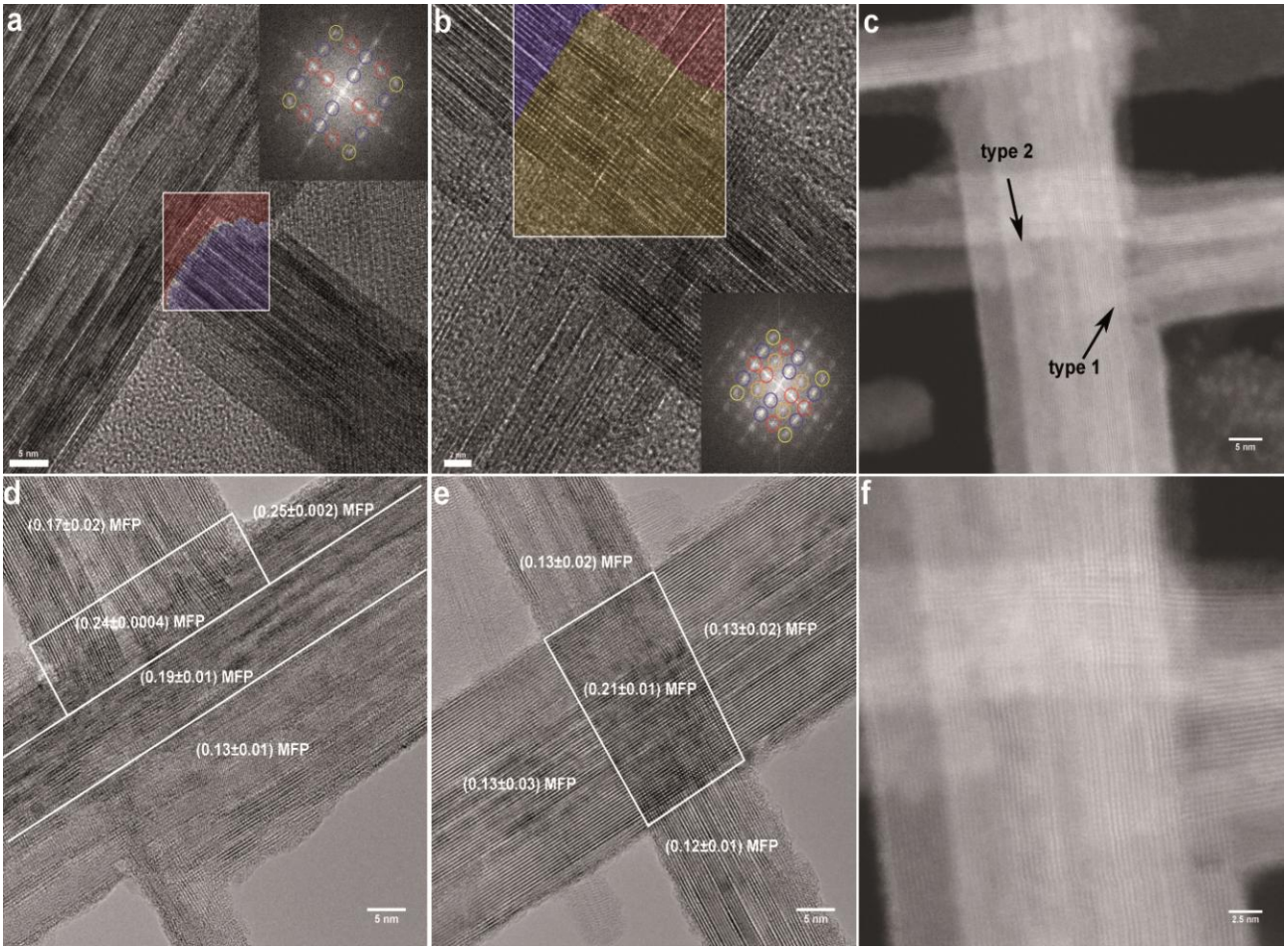

Figure S7. Analysis of the junctions appearing in the network. a) HRTEM image of a T-shaped junction and the corresponding Fast Fourier Transformation (FFT) (inset) of the area marked in the HRTEM image. The color-coding correlates the origin of each spot in the FFT with the respective area in the HRTEM. b) HRTEM image of a crossing, color-coding and FFT like in a), reflexes marked yellow originate from the whole area. c) STEM image including both junction types. Site-specific thickness information were obtained from low-loss EEL spectra. The HRTEM image of the junctions (T-shaped d), crossing e)) include the calculated relative thicknesses in dependence of the mean free path (MFP). f) HAADF image of the two junctions types, showing the preservation of the atomic order at the junctions.

4. Photocatalytic degradation of different dyes

Reference measurements were performed to exclude bleaching of the dyes due to the UV irradiation and to ensure that the decreasing dye concentration results from degradation photocatalyzed by $Nb_3O_7(OH)$. In this regard bleaching experiments with pure dye solutions were performed, the achieved results are shown in Figure S8a-c related to the measured photocatalytic degradation applying $Nb_3O_7(OH)$. To investigate adsorption of dye on the $Nb_3O_7(OH)$ surfaces, the concentration of the used dye solution is compared to the dye concentration of the $Nb_3O_7(OH)$-dye-mixture (Figure S8d).

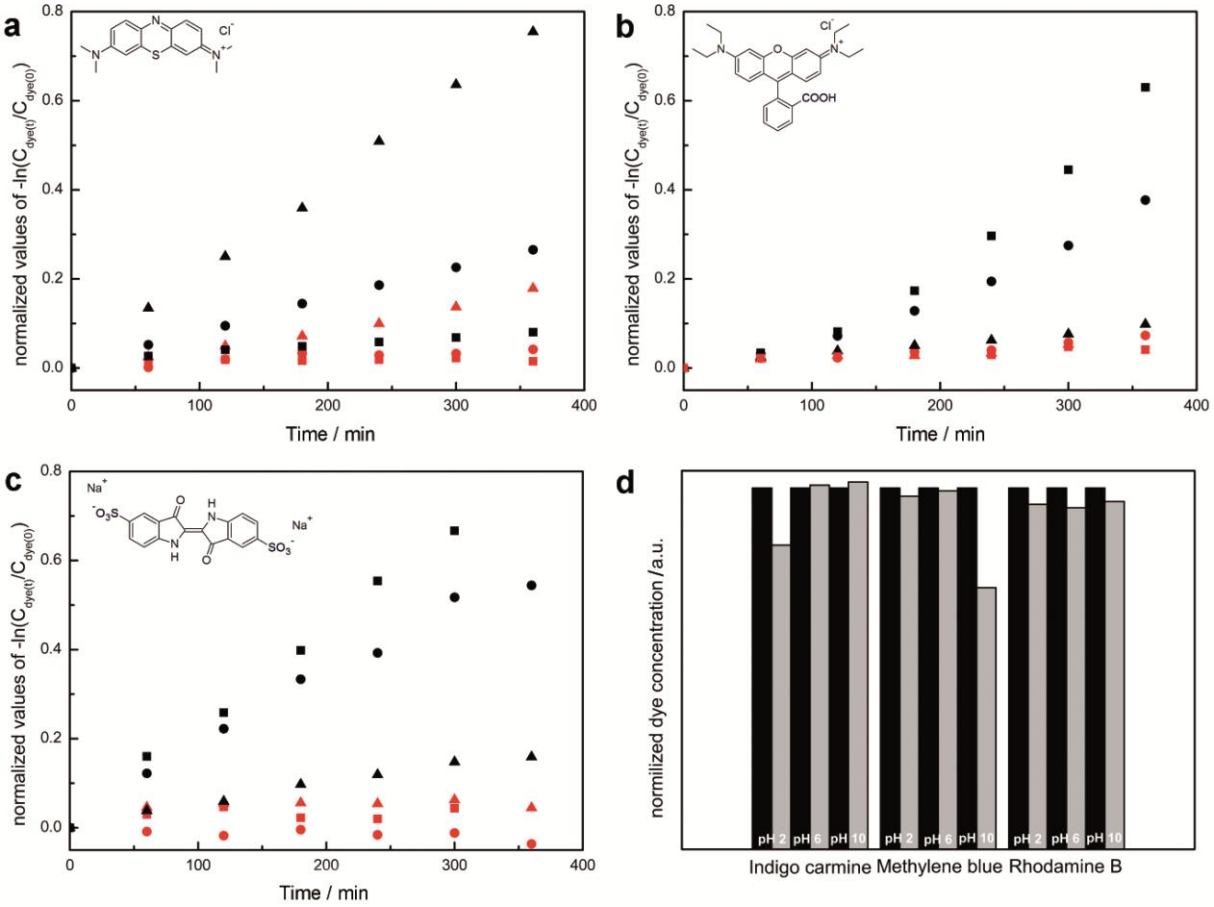

Figure S8. Reference measurements related to the photocatalytic dye degradation measurements. a-c) Bleaching of the dye due to UV irradiation (methylene blue (a), rhodamine B (b) and indigo carmine (c) at different pH-values (pH 2 (■), pH 6 (●) and pH 10 (▲)). The measured bleaching (red symbols) is related to the results of the photocatalytic degradation measurements (black symbols). d) Investigation of dye adsorption onto the $Nb_3O_7(OH)$ surface in dependence of the dye type and the pH value, via measurement of the dye concentration in the solution. The concentration was determined from UV/Vis spectra, the original concentration of the dye is given as black columns, while the dye concentration after incubation with $Nb_3O_7(OH)$ for 1.5 hours is given in light grey.

References

1. J. Tauc, R. Grigorovici, A. Vancu, *Phys. Status Solidi B* 1966, 627.
2. D. Bach, R. Schneider, D. Gerthsen, J. Verbeeck and W. Sigle, *Microsc. Microanal.*, 2009, **15**, 505.
3. P. A. Stadelmann, JEMS-EMS java version, École Polytechnique Fédérale de Lausanne, Lausanne, Switzerland 2004.
4. T. Malis, S. C. Cheng, R.F. Egerton, *J. Electron. Micr. Tech.* 1988, 193.
5. L. Lutterotti, *Nucl. Instrum. Meth. B,* 2010, **268**, 334.